Pflugers Arch - Eur J Physiol (2007) 454:477–494
DOI 10.1007/s00424-007-0223-5

ION CHANNELS

Interaction of syntaxin with a single Kv1.1 channel: a possible mechanism for modulating neuronal excitability

Izhak Michaelevski · Alon Korngreen · Ilana Lotan

Received: 9 October 2006 / Revised: 18 December 2006 / Accepted: 26 January 2007 / Published online: 31 March 2007

Abstract Voltage-gated K^+ channels are crucial for intrinsic neuronal plasticity and present a target for modulations by protein–protein interactions, notably, by exocytotic proteins demonstrated by us in several systems. Here, we investigated the interaction of a single Kv1.1 channel with syntaxin 1A. Syntaxin decreased the unitary conductance of all conductance states (two subconductances and a full conductance) and decreased their open probabilities by prolongation of mean closed dwell-times at depolarized potentials. However, at subthreshold potentials syntaxin 1A increased the probabilities of the subconductance states. Consequently, the macroscopic conductance is decreased at potentials above threshold and increased at threshold potentials. Numerical modeling based on steady-state and kinetic analyses suggests: (1) a mechanism whereby syntaxin controls activation gating by forcing the conductance pathway only via a sequence of discrete steps through the subconductance states, possibly via a breakdown of cooperative movements of voltage sensors that exist in Kv1.1; (2) a physiological effect, apparently paradoxical for an agent that reduces K^+ current, of attenuating neuronal firing frequency via an increase in K^+ shunting conductance. Such modulation of the gain of neuronal output in response to different levels of syntaxin is in accord with the suggested role for Kv1.1 in axonal excitability and synaptic efficacy.

Keywords Kv1.1 · Single channel · Subconductance levels · Syntaxin 1A · Shunting inhibition

Introduction

Kv1.1, a member of the *Shaker* family of K^+ channels, is expressed throughout the central and peripheral nervous system [1, 2]. It is concentrated at juxtaparanodal regions in major PNS and CNS myelinated fiber tracts [3, 4]. In certain non-myelinated CNS axons, it is confined to "septate-like" junctions between two closely opposing axons [5]. Kv1.1 encodes a fast delayed rectifying K^+ channel in heterologous expression systems [6, 7]. Neuronal deficiency [8] or blockade [9] of Kv1.1 impaired learning or increased transmitter release, respectively, implying the role of Kv1.1 in repolarizing the membrane in axons and at synaptic terminals.

Previously, we have shown [10] that Kv1.1 interacts in brain synaptosomes with protein components of the exocytotic machinery: the t-SNARE proteins, syntaxin 1A (syx) and SNAP-25, and the putative Ca^{2+} sensor, synaptotagmin [11–16]. Furthermore, in *Xenopus* oocytes the direct interaction of syx with Kv1.1, alone or in complex with auxiliary Kvβ1.1 subunits, feeds back on the channel function, affecting current amplitudes and fast inactivation of the complex [10]; involvement of G protein βγ subunits (Gβγ) is required for the effect on inactivation [17]. These characteristics of the interaction of a Kv channel with syx are reminiscent of the interaction of N-type Ca^{2+} channels with syx in oocytes [15, 18–20] and "calyx" nerve terminals [21], suggesting that the two presynaptic voltage-gated

Electronic supplementary material The online version of this article (doi:10.1007/s00424-007-0223-5) contains supplementary material, which is available to authorized users.

I. Michaelevski · I. Lotan (✉)
Department of Physiology and Pharmacology,
Sackler School of Medicine, Tel-Aviv University,
69978 Ramat-Aviv, Israel
e-mail: ilotan@post.tau.ac.il

A. Korngreen
Faculty of Life Sciences and the Leslie and Susan Gonda
Interdisciplinary Brain Research Center, Bar-Ilan University,
Ramat-Gan 52900, Israel

channels share a similar mode of interaction with synaptic proteins. Altogether, we have suggested that the interactions of Kv1.1 with the exocytotic proteins might play a role in modulating axonal excitability and synaptic strength.

Our above described electrophysiological characterizations of the interaction between Kv1.1 and syx were done at the level of whole cell currents and thus did not discern between direct interactions that affect single channel behavior and effects on channel expression and/or plasma membrane density. Specifically, we were intrigued by the observation that syx had dual effect on Kv1.1 current amplitudes, depending on its concentration. Initially, we correlated the decreased currents by high syx concentration with a decrease in plasma membrane channel density, arguing that overexpression of syx impaired trafficking of channels to the membrane. Rather, we interpreted the enhanced currents, occurring at low syx concentrations, to reflect the effect of syx on channel gating [10]. However, subsequent experiments (unpublished data) cast some doubts about these resolutions and prompted us to study the effects of syx on single Kv1.1 channel biophysical characteristics. Here, we performed an extensive analysis of single Kv1.1 channels in membrane patches of oocytes expressing Kv1.1, alone or with syx. Modeling of the data elucidates a mechanism whereby syx gains an efficient control over Kv1.1 gating and suggests a mechanism to modulate the gain of neuronal output in response to different levels of syx.

Materials and methods

Oocyte treatment

Frogs were maintained and dissected and the oocytes prepared as described [22]. Oocytes were injected with 7.5–10 ng/oocyes Kv1.1 mRNA alone or together with 0.15 ng/oocyte syx mRNA. Current recordings were performed 2 days after the mRNA injection.

Electrophysiological recordings of single-channel activity

Cell-attached patch clamp technique in *Xenopus* oocytes was performed as described before [23]. Oocytes of which the vitelline membrane was removed were placed in a bath solution containing: 146 mM KCl, 2 mM NaCl, 1 mM $CaCl_2$, 1 mM $MgCl_2$, 0.1 mM EGTA, 10 mM HEPES, pH 8. Patch pipettes were pulled from glass capillary tubing (Warner Instrument Corp.) with 2–5 or 20–40 MΩ tip resistance, for Kv1.1 or Kv1.1+syx patches, respectively. Patch pipettes were filled with solution containing 150 mM NaCl, 2 mM KCl, 1 mM $CaCl_2$, 1 mM $MgCl_2$, 5 mM HEPES, pH 7.5. Single-channel recordings were made in response to step depolarizations from −50 to +70 mV with 20 mV increments at 0.5 Hz. Holding potential was −80 mV. Data was sampled at 20 kHz and filtered with analog Bessel filter at 5 kHz. Amplification was done with Axopatch 200 amplifier; acquired analog signal was digitized with DigiData 1200 B converter, recorded with clampexdd and analyzed in Clampfit 9.2 (pClamp, Axon Instruments Inc.). Prior to event detection analysis data was filtered at 3 kHz with digital Gaussian filter (additional 1.5 kHz filtering was used at −50 mV). The capacitance and leak currents were subtracted using averaged 3–5 empty sweeps. Event detection was performed using algorithm built in pClamp9.2 software.

Data analysis of single channels

Conductance levels were derived from amplitude histograms built up from pClamp9.2 generated event list. The histograms were fitted with a multicomponential Gaussian probability function, using Levenberg–Marquardt method (precision criterion for convergence was set to 10^{-6}) with the sum of square errors minimization technique. To enhance Gaussian components, event number (y-axis of histograms) was transformed into square root. Initial event analysis was based on two states (closed and open) detection. However, due to the appearance of subconductance states, each conductance was set separately, mutually excluding simultaneous existence of other conductance states.

Open probabilities (P_o) for each conductance were calculated separately from the event list as P_o of independent events for each conductance state. The summarized open probabilities (ΣP_o) were calculated by summation of P_o values of all conductance states.

For generation of open and closed time histograms, the Sigworth's dead-time (T_d) parameter was used (T_d=0.179/f_c where f_c is the cut-off frequency of the analysis filtering). Open and closed times' analyses were performed in the −30 to +70 mV potential range. No kinetic analysis was performed at −50 mV due to low signal-to-noise ratio. Closed and open times were binned using variable binning. Minimum-duration of bin was set to be the dead-time used for the event detection. Logarithmic binning of the dwell times and event number square root was used to plot histograms. Multi-exponential distributions were fitted with multi-exponential log–probability fitting function:

$$pdf = \sum_{i=1}^{n} P_i \exp\left[(\ln(t) - \ln(\tau_i)) \exp(\ln(t) - \ln(\tau_i))\right] \quad (1)$$

Where P_i is the probability of τ_i dwell time, *pdf* is the probability density function and n is the number of

exponents applied for fitting. Simplex search algorithm with maximum likelihood minimization method calculated with maximal 20000 iterations to a 1*e*−06 precision was used for fitting. The obtained probability density function (*pdf*) curve was superimposed over the histograms. Using dwell time constants and their probabilities, mean open and closed times were calculated to reconstitute P_o obtained from the event list analysis (see Results).

First latencies calculated by constructing cumulative histograms and one-exponential rise function were used to derive mean first latency values.

A Hidden Markov Model (HMM)-based simulation was performed using QUB software package (for details see Supplementary information). The predicted model was simulated at 20 kHz. Kinetic constants and unitary amplitudes of each level with the corresponding standard deviations were supplied according to the experimental data. The macroscopic current was simulated using a sampling rate of 20 kHz with one segment, containing 8000 samples.

The voltage dependence of the state transitions rate-constants was estimated by one-exponential decay or rise functions for the Kv1.1 group. For the Kv1.1+syx group we used one-exponential product function:

$$k = k_0\left(1 - e^{-V/x_a}\right)\left(e^{-V/x_d}\right) + const \tag{2}$$

Where x_a and x_d are voltage dependence constants for the rising and decaying components, correspondingly; for each component:

$$x = \frac{RT}{zF} \tag{3}$$

Where R is the universal gas constant, F is the Faraday constant, T is absolute temperature in Kelvin, and z is number of elementary electric charge.

Electrophysiological recording of cell-attached macro-patch currents

Solutions and equipments were as for the single-channel analysis. Low resistance electrodes (0.5–2 MΩ) were used.

Current–voltage protocol: Membrane potential was stepped from holding potential of −80 mV to 200 msec depolarizing potentials from −80 to +75 mV with 5 mV increments. Inter-episode time was 2 s. Leak currents measured by a 200 msec step to −90 mV were subtracted.

Deactivation protocol: Following a 100 msec depolarizing step to +50 mV, the membrane potential was repolarized for 90 msec to test pulses ranging from −45 to −140 mV. Inter-episode time was 2 s. Leak currents measured by a 30 msec step to −90 mV were subtracted.

Analysis of macro-patch current traces and simulations

Activation and deactivation current traces were fitted to the equation:

$$I(t) = I_\infty - (I_\infty - I_0)e^{-t/\tau} \tag{4}$$

Where t is time, I_∞ is the steady-state current, I_0 is current at t=0, and τ is time constant of the exponential relaxation in the model. The normalized conductance was fitted to a Boltzmann equation:

$$\frac{G}{G_{\max}} = \frac{1}{1 + \exp\left(-\frac{V - V_{1/2}}{a}\right)} \tag{5}$$

Where $G/G_{\max}$ is the normalized conductance, V is the membrane potential, $V_{1/2}$ is voltage at which the conductance is activated to half its maximal value, and a is the slope factor. All the simulations of the action potential were carried out in a single compartment model using NEURON 5.6 [24] on a PC with SuSE Linux 9.1 with an integration time step of 25 μs.

Results

Steady-state analysis of single channel properties of Kv1.1, alone and in the presence of syx

Single channel recordings of Kv1.1 expressed in *Xenopus* oocytes were performed, using the cell-attached configuration of the patch clamp technique, 2–3 days after the injection of Kv1.1 mRNA. Co-injection of syx mRNA was used to assess syx effects. Analysis was performed only on patches displaying no overlapping openings during the whole period of recording, arguing for the presence of a single channel in the patch. Recordings were performed at potentials ranging from −50 to +70 mV with 20 mV increments. Four patches expressing Kv1.1 alone (hereafter: Kv1.1 patches) and six patches co-expressing Kv1.1 with syx (hereafter: Kv1.1+syx patches) were selected for analysis. Three phenomena were apparent upon visual inspection of the records (representative consecutive sweeps evoked by depolarizing steps to different voltages for Kv1.1 and Kv1.1+syx patches are shown in Fig. 1). Firstly, at −50 mV channel activity was already detected in Kv1.1+syx but not in Kv1.1 patches. Secondly, single channel current amplitudes were heterogeneous, pointing out to the existence of subconductance states at all tested potentials in both Kv1.1 and Kv1.1+syx patches. Thirdly, silent periods were more frequent and more prolonged in Kv1.1+syx vs Kv1.1 patches.

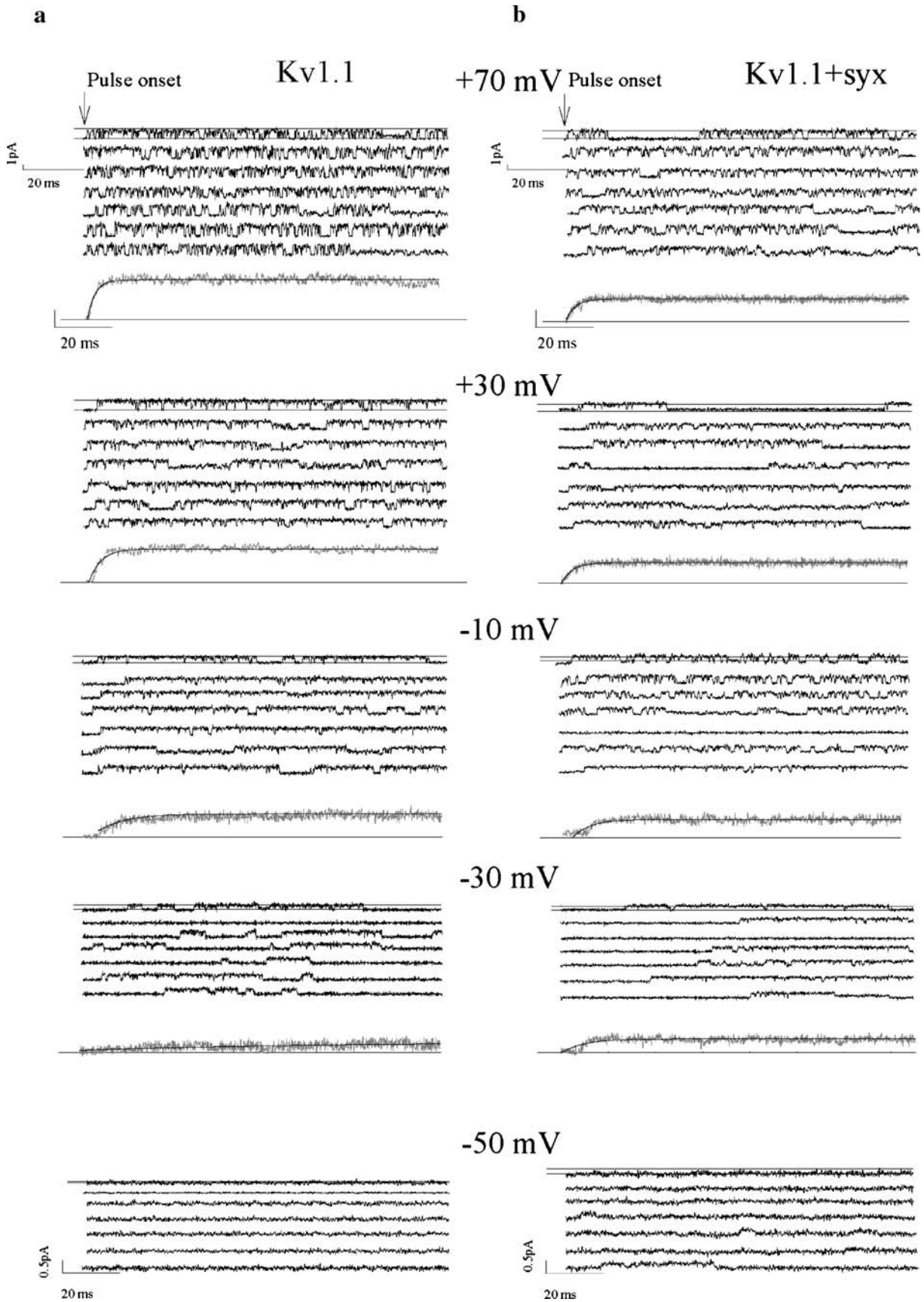
a
b
Kv1.1
Kv1.1+syx
Pulse onset
Pulse onset
+70 mV
1pA
20 ms
20 ms
20 ms
+30 mV
-10 mV
-30 mV
-50 mV
0.5pA
20 ms
20 ms

◀ **Fig. 1** Consecutive traces at different potentials (*as denoted*) and the corresponding ensemble averaged currents (*below the traces*). **a** Kv1.1 patches. **b** Kv1.1+syx patches. Note the different amplitude scaling at −50 mV

Analysis of unitary channel conductance

Statistical analysis of closed and open event distribution revealed the existence of subconductance levels, in addition to a full conductance level, F, in both Kv1.1 and Kv1.1+syx patches (see in Fig. 7b). Two subconductances, S1 and S2, lower and higher than 50% of F, respectively, were defined (see for Kv1.1 patches at extreme potentials in Fig. 2a–c). The difference between the unitary current amplitudes at S2 and F levels was small but consistent (see values in Fig. 2d). However, in order to ascertain that S2 and F were distinct levels and S2 was not an artifact of fast channel flickering that could be missed by our sampling rate, we performed additional filtering of the current at 1000 Hz and 500 Hz. Despite the significant under-sampling of the record, the difference in the unitary current amplitude between S2 and F levels was conserved (Fig. 2b). We acknowledge that precision of measurements at potentials near the channel activation (e.g., Fig. 2c at −30 mV) is less strict, hence it was more difficult to resolve S2 from F. However, only a four componential Gaussian equation can describe appropriately the all point histogram with tiny but well-shaped fourth component (corresponding to F; see Fig. 2c, inset). Unitary channel conductance (γ) for each conductance (Fig. 2d) was evaluated from the corresponding current–voltage (i–V) plot (Fig. 2c). At all three conductances, γ values were lower in the presence of syx; nevertheless, at S1 the effect of syx was not statistically significant (Fig. 2d).

Open probability analysis

Analysis of the open probability (P_o) of the channels was performed for each conductance separately, in both Kv1.1 and Kv1.1+syx patches, analyzing diaries of P_o for openings at each level at all tested voltages (representative diaries are displayed in Supplementary Figs. 1, 2 and 3). Voltage dependence analysis of averaged P_o values measured for the S1 subconductance did not show significant changes in P_o over the whole range of voltages tested, in each one of the groups; nonetheless, channel openings were apparent at more negative potentials in the presence of syx (Fig. 3a). Consequently, application of the Boltzmann charge–voltage fit equation showed very small slope factor values (1.47 mV for Kv1.1 and 1.78 mV for Kv1.1+syx patches), corresponding to high charge cooperativity for the S1 level. Two major differences between the Kv1.1 and Kv1.1+syx groups were prominent at S1. Firstly, syx shifted the half P_o potential, $V_{1/2}$, to the left by about 19 mV (from −34.36 mV in Kv1.1 to −53.49 mV in Kv1.1+syx patches). Secondly, syx led to about a twofold decrease of P_o in the range of membrane potentials −30 to +70 mV (Fig. 3a).

Voltage dependence analysis of averaged P_o values measured for the S2 subconductance (Fig. 3b) showed a leftward shift by about 9 mV of $V_{1/2}$ in (from −21.18 mV to −30 mV) and an increase in slope factor by about 9.5 mV (from 5.48 mV to 14.18 mV), upon syx co-expression, indicating lower voltage sensitivity in the presence of syx. Also, syx decreased the averaged P_o values at S2 in the voltage range of −10 mV to +70 mV by about 30%. Voltage dependence analysis of averaged P_o values measured for the F subconductance revealed that syx decreased P_o by about 30%, but did not significantly affect $V_{1/2}$ or the slope factor (−31.2 mV and 6.23 mV for Kv1.1 patches and −33.28 mV and 7.52 mV for Kv1.1+syx patches, respectively; Fig. 3c).

To obtain the complete open probability behavior of the channel, we performed per-trace summation of the P_o values for each level over all patches and calculated the total P_o (ΣP_o, summarized P_o) at each of the tested potentials (representative P_o histograms are presented in Supplementary Fig. 4). Voltage dependence analysis of ΣP_o values showed that syx shifted $V_{1/2}$ to more hyperpolarized potentials, increased the slope factor of activation and decreased ΣP_o by about 30% in the range of −10 mV to +70 mV (Fig. 3d).

Reconstitution of the macroscopic conductance

We further sought to reconstitute the voltage-dependent behavior of the macroscopic conductance (G) of Kv1.1 and Kv1.1+syx on the basis of the derived values of P_o and γ. In the case of a channel having a single conductance, G can be calculated using the equation:

$$G = n\gamma P_o \tag{6}$$

Where n is the number of channels. In the case of multiple conductances, as in our case, G can be calculated using the equation:

$$G = n\sum_i \gamma_i P_{o_i} \tag{7}$$

Where γ_i and P_{o_i} correspond to the ith conductance. Thus, reconstitution of G (for n=1000 channels) showed about a twofold decrease in the Kv1.1+syx group at positive potentials (Fig. 4a). The predicted steady-state activation curve showed a left-shift of the half-activation potential, $V_{1/2}$, by about 10 mV and a slope factor increase by about 4 mV (Fig. 4b–d). The contribution of each ith conductance (c_i) to G can be calculated using the equation:

$$c_i = \gamma_i P_{o_i} \Big/ \sum_i \gamma_i P_{o_i} \tag{8}$$

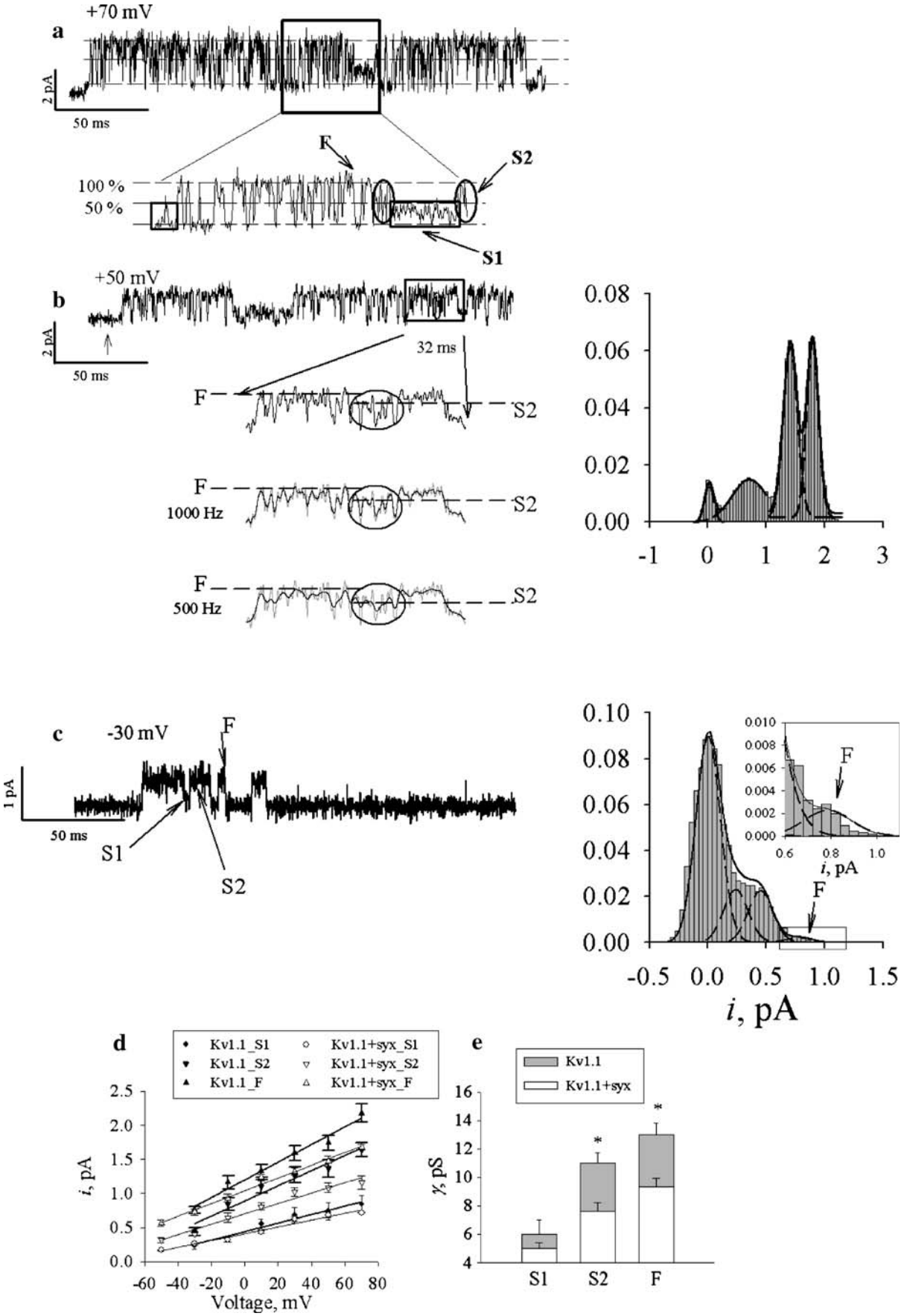
a
+70 mV
2 pA
50 ms
F
S2
100 %
50 %
S1
b
+50 mV
2 pA
50 ms
32 ms
F
S2
1000 Hz
500 Hz
0.08
0.06
0.04
0.02
0.00
-1
0
1
2
3
c
-30 mV
1 pA
50 ms
S1
S2
0.10
0.08
0.06
0.04
0.02
0.00
-0.5
0.0
0.5
1.0
1.5
i, pA
0.010
0.008
0.006
0.004
0.002
0.000
0.6
0.8
1.0
d
Kv1.1_S1
Kv1.1_S2
Kv1.1_F
Kv1.1+syx_S1
Kv1.1+syx_S2
Kv1.1+syx_F
i, pA
Voltage, mV
e
Kv1.1
Kv1.1+syx
γ, pS
S1
S2
F

◀ **Fig. 2** Analysis of single channel conductances in Kv1.1 and Kv1.1+syx patches. **a** A representative trace recorded at +70 mV in a Kv1.1 patch with a single channel. *Blown up square* contains, in addition to the full conductance (F) two subconductances, S2 and S1, shown in *circles* and *squares*, respectively. **b** *Left panel*: Low-pass filtering shows that S2 and F are two distinct conductances. A 32 ms episode blown up from a representative trace recorded at +50 mV was further filtered digitally as indicated at the two bottom traces. *Gray* (*dotted*) and *black traces* depict unfiltered and filtered data, respectively. *Circles* depict a cluster of S2 events. *Dashed lines* depict S2 and F conductances. *Right panel*: Amplitude distribution of all the detected conducting levels (close, S1, S2 and F) at +50 mV. *Solid line* depicts a multi-Gaussian function fitting value applied to the entire distribution, whereas *dashed lines* show an individual Gaussian component corresponding to each conducting level. **c** *Left panel*: A representative single channel current trace recorded at −30 mV in a Kv1.1 patch showing the conductance levels. *Right panel*: Per event amplitude histogram shows a four-component multiple-Gaussian distribution (as in **b**, *right panel*). "F" denotes the full conductance component framed in the *rectangle*. *Inset*: Magnification of the rectangle. **d** Unitary current amplitudes (*i*) plotted vs membrane potential in Kv1.1 (*solid symbols*) and Kv1.1+syx (*open symbols*) patches at the three conductances: S1 (*solid circles*), S2 (*solid inverted triangles*) and F (*solid triangles*). The averaged data was derived from four Kv1.1 and six Kv1.1+syx patches. *Solid lines* depict a fit to the polynomial equation $i = \gamma V +$ const where γ denotes the unitary conductance for a conductance level. Because the SNR was low at −50 mV, the amplitudes of the manually detected events for each level were corrected according to the extrapolation of the polynomial equation noted above. **e** Derived γ values for all conductances for Kv1.1 (*white bars*) and superimposed Kv1.1+syx (*gray bars*). *$p<0.01$

The c_i values for each of the conductances for the K1.1 and Kv1.1+syx groups were plotted against the tested voltages (Fig. 4e). In both groups, in the potentials range between −10 and +70 mV, S2 and F had similar and major contributions to G, whereas at more negative potentials, the contribution of S1 increased significantly (especially in Kv1.1+syx). Differences between the two groups were prominent only at negative potentials, where the c_i values exhibited high voltage sensitivity (reflected in the corresponding k_c constants shown in Fig. 4e; see legend).

Kinetic analysis of P_o of Kv1.1, alone and in the presence of syx

To understand the differences in the P_o values between the groups, we performed kinetic analysis to derive open and closed dwell times at each of the conductances in each of the groups. Open time distributions for each level were fitted by a sum of two or three exponential functions, as required (Supplementary Fig. 5). The derived open time constants were used for further analysis of mean open times, since open time constant (τ) equals mean open time (t) only in the case of single exponential distribution. In a multi-exponential distribution, as is the case for each level, the mean open time of level X (t_x) can be calculated as the sum of mean open times of all the components using the equation:

$$t_x = \sum_j t_j = \sum_j \tau_j \, p_j \qquad (9)$$

Where p_j is the probability (or weight; see the "Materials and methods" section), τ_j is the time constant and t_j is the

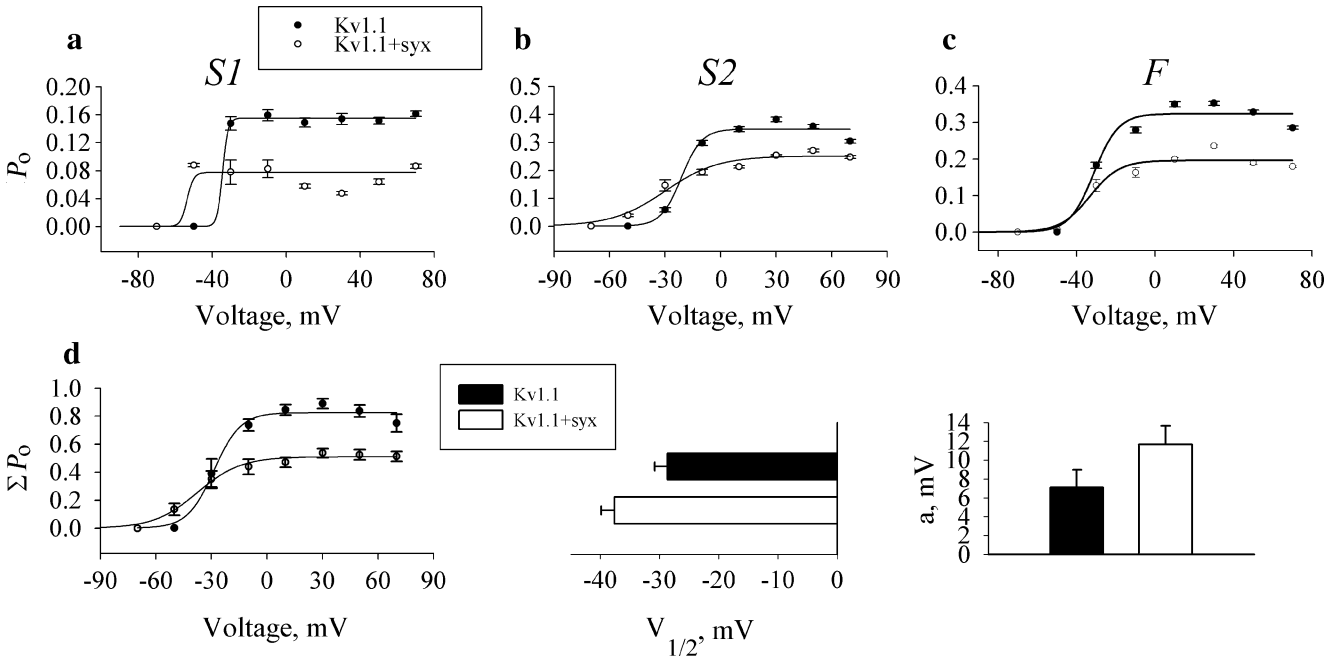

Fig. 3 Voltage dependence of P_o behavior in each of the conductances, separately and pulled together. P_o values in S1 (**a**) S2 (**b**) and F (**c**). **d** Total P_o values, (ΣP_o, *left panel*), and the derived parameters: half-open probability potential ($V_{1/2}$, *middle panel*) and slope factor (a, *right panel*). Data presented is averaged over four and six patches of Kv1.1 and Kv1.1+syx, respectively

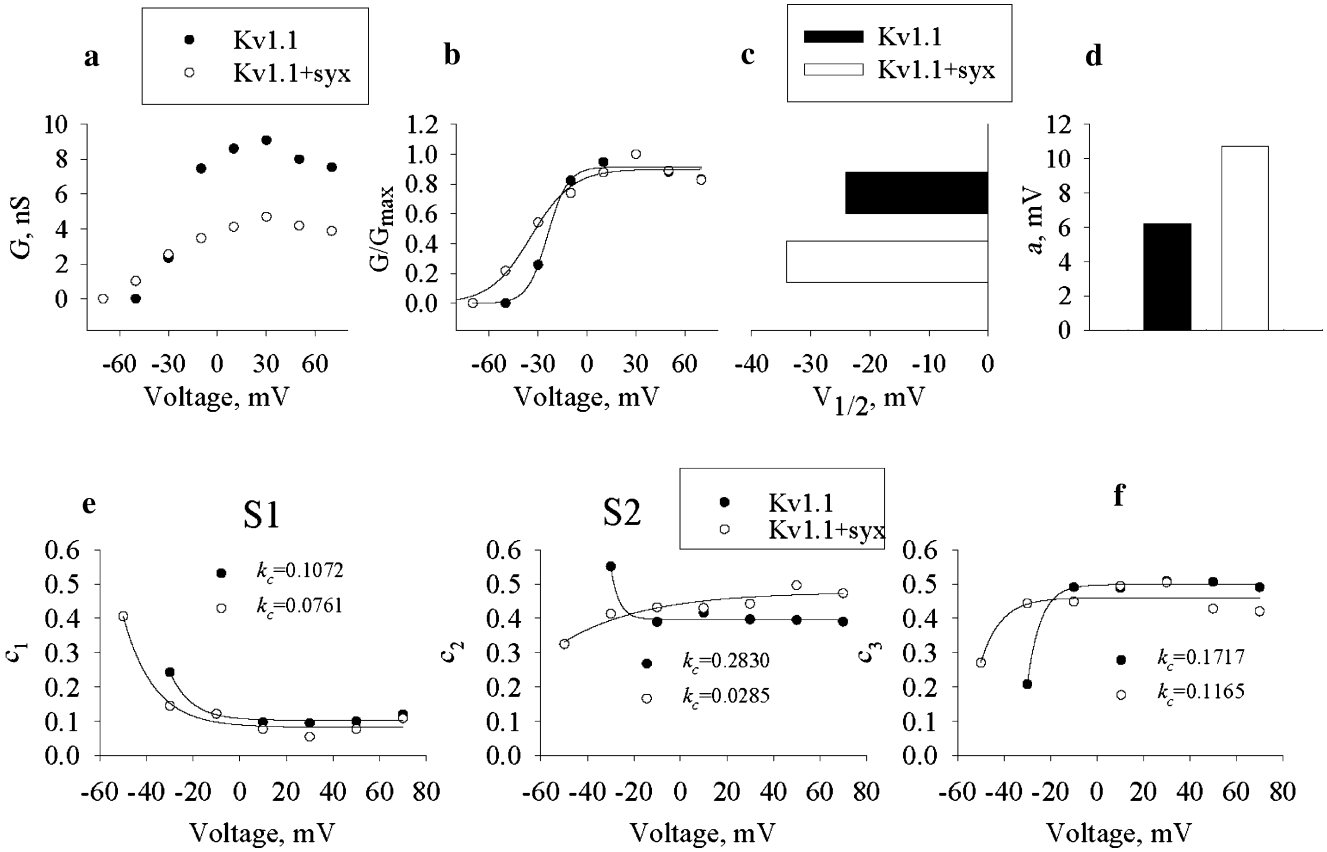

Fig. 4 Macroscopic conductance (G) in Kv1.1 and Kv1.1+syx groups reconstituted from summarized P_o values and the relative contributions of the conductances. **a** G values calculated using Eq. (6) for 1,000 channels plotted against tested voltages. **b** Steady-state activation curves derived from data in **a** fitted with one-componential charge–voltage Boltzmann equation (*solid lines*). **c**, **d** The derived half-activation voltages ($V_{1/2}$) and slope factor (a), respectively. **e**, **f** Con><?downtribution of each conductance (as indicated above the graphs) to G at all tested voltages calculated using Eq. (8). *Solid circles* depict Kv1.1 alone and *open circles* depict Kv1.1+syx. To estimate voltage dependence, the data were fitted (*solid lines*) with either one-exponential rise or decay functions: $c=c_0*exp\ (-k_c*V)+const$ or $c=c_0*(1-exp(-k_c*V))+const$, respectively where c is the contribution of the corresponding conductance at a certain voltage (V). The derived k_c values are proportional to the charge transfer in each conductance ($k_c=zF/RT$)

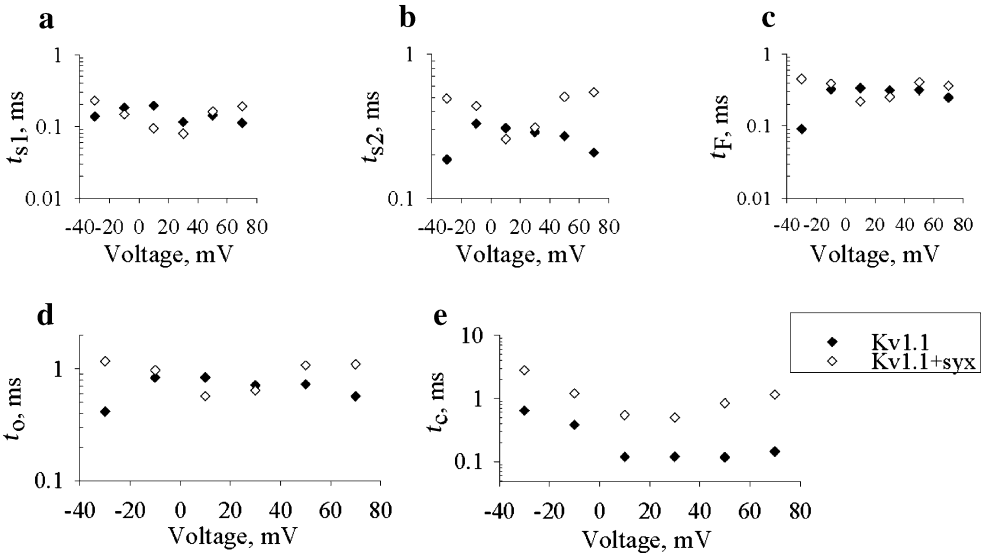

Fig. 5 Kinetic parameters derived from open and closed time distributions. Voltage dependence of the mean open time (t_x) for S1 (**a**), S2 (**b**) and F (**c**), correspondingly. **d**, **e** Voltage dependence of total mean open times (t_o) and mean closed dwell times (t_c), correspondingly. *Closed* and *open symbols* represent Kv1.1 and Kv1.1+syx groups, respectively

mean open time of the *jth* component. Namely, t_j is the contribution of τ_j to the mean open time of a given level X, t_x. The voltage dependence of the different time constants and their probabilities at each of the levels for Kv1.1 and Kv1.1+syx is described in Supplementary information and shown in Supplementary Fig. 6. Figure 5 shows the derived mean open times at each of the levels. In S1, the mean open times (t_{s1}) did not differ significantly between Kv1.1 and Kv1.1+syx (Fig. 5a) and could not account for the observed difference in P_o at S1 between the groups (Fig. 3a). In S2, the mean open times (t_{s2}; Fig. 5b) were quite similar between the groups at the −10 to +30 mV range and at extreme potentials they diverged and could not account for the observed lower P_o of Kv1.1+syx at S2 (Fig. 3b). In F, the mean open time values (τ_F; Fig. 5 *F*C) were quite similar between the groups at all potentials, except at

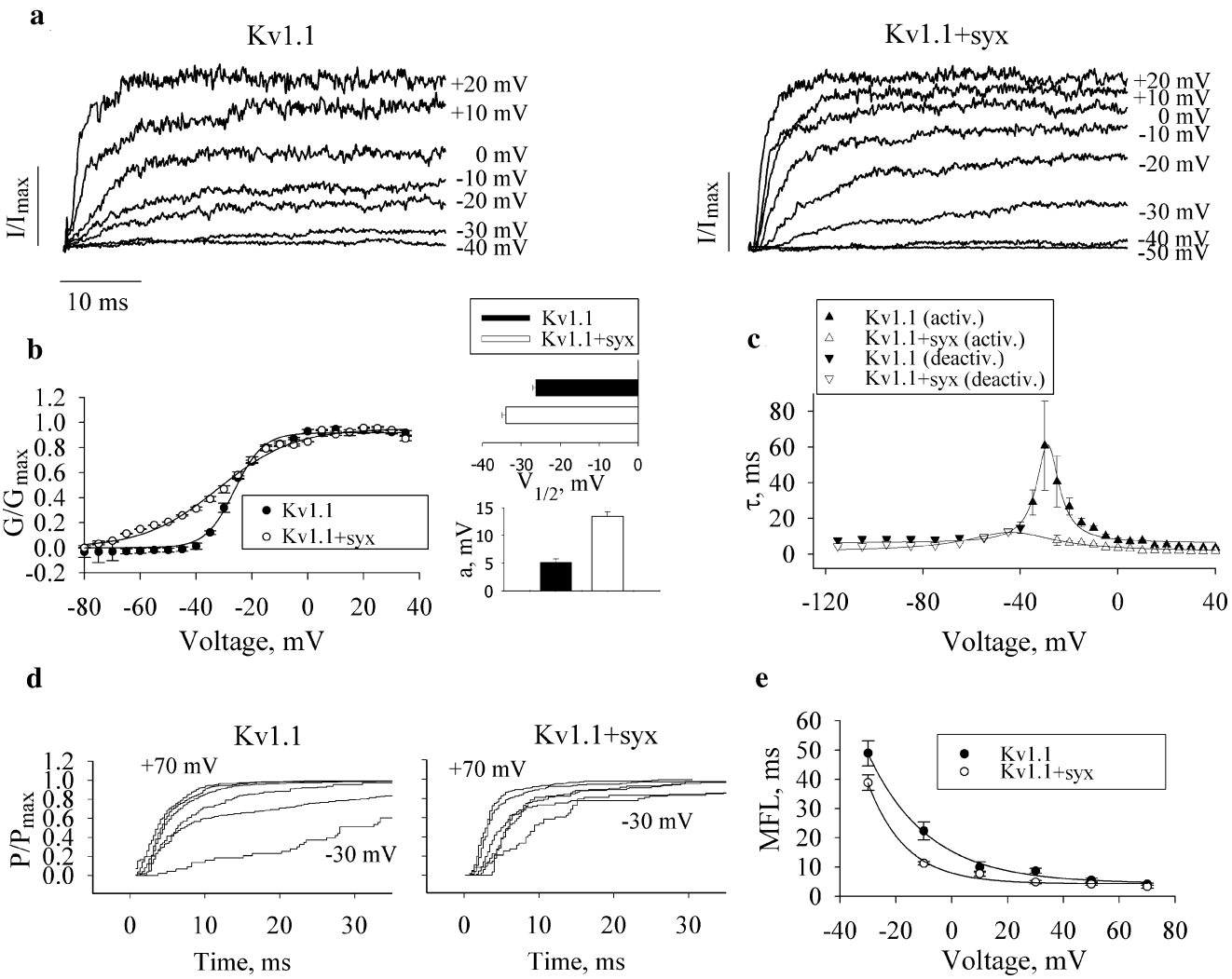

Fig. 6 Corroboration of steady-state activation and kinetic behavior in single channel patches of Kv1.1 and Kv1.1+syx by analysis of macro-patch currents. **a** Representative current traces recorded from two macro-patches from oocytes expressing Kv1.1 alone (*Kv1.1*) or with syx (*Kv1.1+syx*), in response to the indicated voltages. Because current amplitudes were variable among different macro-patch recordings (due to different distribution of the channels on the cell surface), the analyzed amplitudes were normalized to the maximal amplitude observed in the measured range in each group. **b** *Left panel*: averaged steady-state activation curves obtained from macro-patch recordings (three and six patches in Kv1.1 Kv1.1+syx groups, respectively). The *continuous lines* are one-componential Boltzmann charge–voltage fit. *Right panels:* half activation voltage ($V_{1/2}$) and slope factor (a) values derived from the fitted curves, respectively. G was calculated from Ohm's equation: $G = I/(V - E_{rev})$. E_{rev} was determined to be −98 mV, the reversal potential of tail currents. **c** Superimposed time constants of activation (*activ.*) and deactivation (*deactiv.*) values of macro-patch currents from the above Kv1.1 (*open symbols*) or Kv1.1+syx (*closed symbols*) patches. Deactivation time constants were calculated according to current–time exponential decay function: $I=I_{max}\exp(-t/\tau)$. The time constants were fitted (*solid lines*) to the equations: $\tau=6.3+1750/((V+29)^2+32)$ for Kv1.1 and $\tau=1.7+5350/((V+44)^2+506)$ for Kv1.1+syx groups. **d** Normalized open probabilities obtained from cumulative histograms of first latency (with 0.3 ms bins) derived from analysis of more than 250 traces from Kv1.1 (*left*) and about 500 traces from Kv1.1+syx (*right*) patches in the voltage range from −30 to +70 mV. **e** MFL values for Kv1.1 and Kv1.1+syx (*open* and *closed circles*, respectively; *solid lines* depict exponential fits) at different potentials

−30 mV where that of Kv1.1 was significantly smaller, and could not account for the observed lower P_o of Kv1.1+syx at F (Fig. 3c). Total mean open time of the channel (t_o) is the sum of the mean open times at all levels (t_{s1}, t_{s2} and t_F). Figure 5d reveals that coexpression of syx shortened t_o in the +10 to +30 mV range, prolonging it towards more positive and negative potentials. Evidently, analysis of open time distribution did not uncover the cause for the observed decrease in total P_o in the presence of syx (Fig. 3d).

Closed time distributions were fitted by a sum of two to five exponential functions, as required (Supplementary Fig. 7). The derived closed time constants for Kv1.1 and Kv1.1+syx are summarized in Supplementary Tables 1 and 2, respectively. Figure 5e shows that in the presence of syx there was a substantial prolongation of the derived mean closed times (t_c) at all potentials. This phenomenon seems to be the main factor accounting for the lower P_o in the presence of syx.

We then reconstituted P_o from the mean open (t_o) and closed (t_c) times using the equation:

$$P_o = \frac{t_o}{t_o + t_c} \tag{10}$$

The reconstituted P_o values at all voltages matched satisfactorily the corresponding values obtained by the event list analysis for Kv1.1 and Kv1.1+syx (Supplementary Fig. 7).

Relationship between macro-patch and single channel currents

The voltage dependence of the steady-state activation of cell-attached macro-patch currents was determined in the presence and absence of syx (Fig. 6a,b). Syx shifted $V_{1/2}$ by ~−10 mV and increased the slope factor by ~7 mV. These effects of syx on macro-patch currents were similar to those predicted by the single channel analysis (Fig. 4b). Further, time constants of current activation of macro-patch currents were analyzed using Eq. (4). In the presence of syx the activation time constants decreased for most of the voltage range examined, with prominent decreases observed between −30 mV to −10 mV (Fig. 6c). These data were compared with corresponding data derived from single-channel activation kinetics' mean first latency (MFL) analysis. The first latency cumulative histograms, obtained at the different voltages in Kv1.1 and Kv1.1+syx patches (Fig. 6d), showed good correlation with corresponding superimposed normalized ensemble currents and normalized macro-patch currents (not shown). Comparative analysis of the derived MFL values between the Kv1.1 and Kv1.1+syx groups showed that at negative potentials the MFL values were significantly lower in the presence of syx (Fig. 6e). Taken together, the steady-state and kinetic parameters derived from single-channel analysis, correlated well with those derived from multi-channel analysis. Analysis of deactivation time constants, using exponential decay fit of macro-patch current tails (not shown), showed that syx did not affect the deactivation time constants (Fig. 6c).

Fig. 7 A model simulating Kv1.1 behavior in the presence and absence of syx, based on a Hidden Markov Model (HMM). **a** Simplified model of state transitions incorporating all observed states. Notifications: α and β are rate constants for all closed states transitions to the last closed state before the opening (forward and backward, respectively); k_{ij} denotes a rate constant of a state transition (from *i*th to *j*th states) among the last closed state and all open states: *0*: closed (C_n); *1*: S1, *2*: S2, *3*: F state. **b** Amplitude distribution histograms of simulated and experimental data for Kv1.1 and Kv1.1+syx groups from −30 to +70 mV. Simulated data was analyzed in QUB software package using constant binning with 50 bins per histogram. 100 traces at each potential in each group were used to obtain data. Experimental data was analyzed in Clampfit with variable binning (of 0.05–0.07 pA width). Data from 4 patches (about 150–200 traces) and 6 patches (about 350–400 traces) of Kv1.1 and Kv1.1+syx groups, respectively. *Solid lines* depict a multi-Gaussian function fitting value applied to the entire distribution, whereas *dashed lines* show each Gaussian distribution separately. **c** Macroscopic current traces derived from the state model after final optimization of all single channel parameters for Kv1.1 and Kv1.1+syx. **d** Macroscopic conductance of the simulated macroscopic currents. **e** Steady-state activation curve of the simulated macroscopic conductances. **f** Simulated MFL values derived from corresponding cumulative histograms of first latency (not shown) of the simulated single channel currents

Channel model that simulates Kv1.1 behavior in the presence and absence of syx

A simulation of the channel's state transitions in the presence and absence of syx was performed, using the corresponding experimentally obtained kinetic parameters, thereafter to compare the predicted unitary amplitude distributions with the experimental distributions. A simulation based on a Hidden Markov Model (HMM) was performed considering each conductance state as a specific state. Two extreme closed states were introduced: the closed state before the voltage sensor movement (C_1) with 100% initial occupancy, and the last closed state before the channel opening (C_n). Kinetic constants for conformation changes between $C_1 \forall C_n$ and $C_n \forall C_1$ (α and β, respectively) were derived from MFL values according to the equation:

$$\alpha/\beta = \frac{x}{x^{*}MFL} \tag{11}$$

Where α and β are the summed up kinetic constants of $C_1 \forall C_n$ and $C_n \forall C_1$, respectively; x is ratio coefficient (in spite of no mathematical sense, it makes sense in the case of transition probabilities. Since the model includes multi-

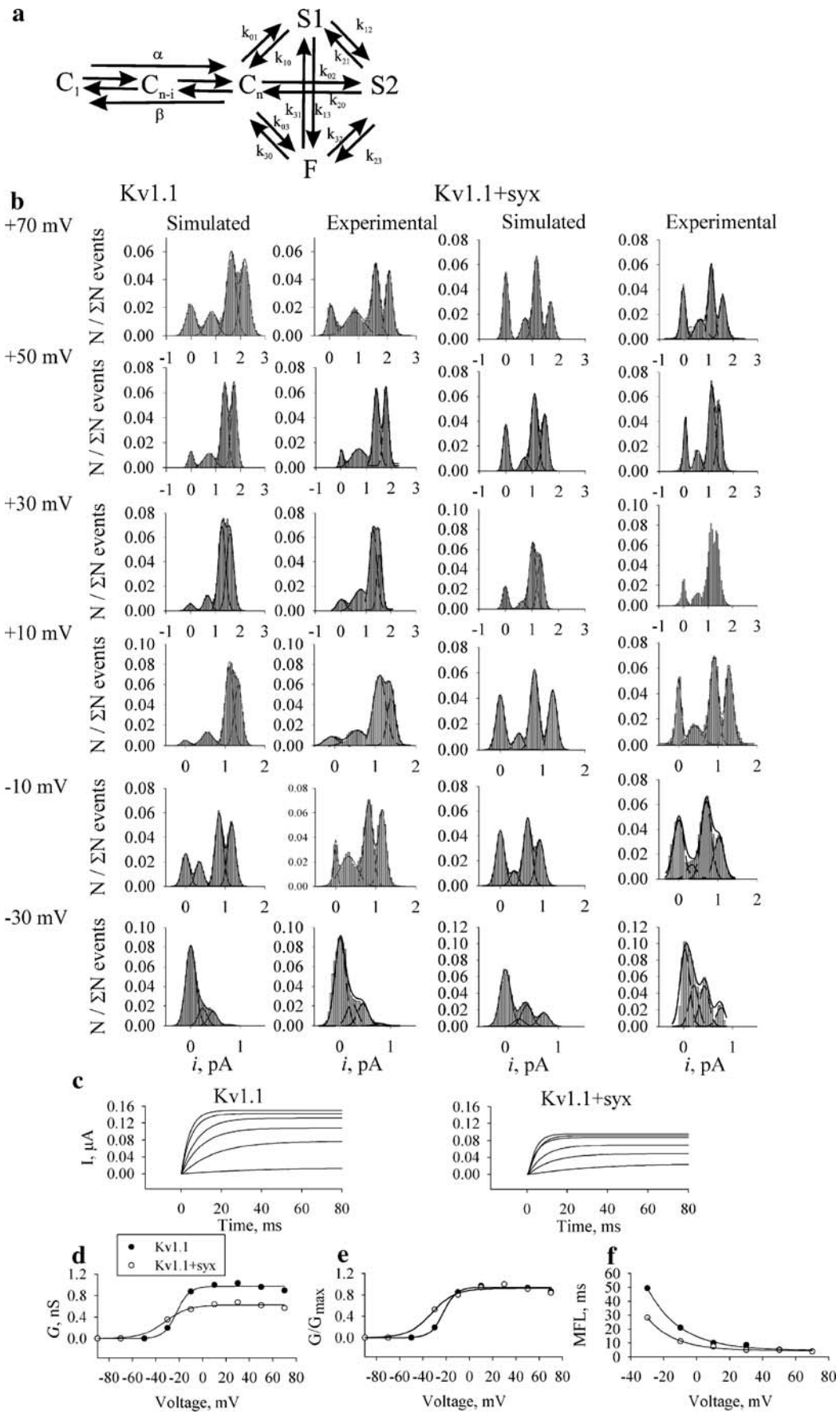
a
S1
S2
F
C1
Cn-i
Cn
α
β
b
Kv1.1
Kv1.1+syx
Simulated
Experimental
+70 mV
+50 mV
+30 mV
+10 mV
-10 mV
-30 mV
N / ΣN events
i, pA
c
Kv1.1
Kv1.1+syx
I, μA
Time, ms
d
Kv1.1
Kv1.1+syx
G, nS
Voltage, mV
e
G/Gmax
Voltage, mV
f
MFL, ms
Voltage, mV

state transitions, channel reaching the state C_n has different probability to return to the state C_1 if there were no additional open states. Consequently, the rate of a single channel reaching the state C_n alters the probability of the further opening even if its ratio to $C_n \forall C_1$ transition remains unchanged). Kinetic constants for state transitions between all states were based on the experimental data according to the equation (from [25]):

$$k_{ij} = \frac{f_{ij}}{t_i} \tag{12}$$

Where k_{ij} is the kinetic constant describing the transition from the ith to the jth state. t_i is the mean dwell time in state i and f_{ij} is the probability of all transitions leaving state i that end in state j. This equation uses the mean dwell times of the states and ignores the fact that each dwell time constant is the real kinetic characteristic for the energy transition. Consequently, the obtained model is statistical and not kinetic. The obtained rate constants (see below) were applied to the model shown in Fig. 7a, using corresponding unitary current amplitudes and their standard deviations at each potential for each conductance. The obtained current was idealized and the kinetic constants were optimized using the method of maximal interval likelihood rate estimation built-in into the QUB software package [26, 27]. The optimized kinetic constants were used in a second round of the simulation to idealize the obtained data.

To assess the model, several model-derived simulated data were challenged by comparing them with the corresponding data derived from single channel analysis. Firstly, comparison of the unitary amplitude distributions derived from simulated and experimental data event list analyses showed high resemblance at all potentials, especially at more positive potentials (Fig. 7b), in both Kv1.1 and Kv1.1+syx groups (for further discussion see Supplementary information). Secondly, comparison of simulated currents (Fig. 7c–e) with the corresponding macroscopic conductances, reconstituted on the basis of single-channel analysis (Fig. 4a–d), showed high resemblance in both groups. Finally, comparison of MFL values, derived from cumulative histograms of first latency of the simulated unitary currents (Fig. 7f) with the corresponding values obtained experimentally (Fig. 6e) showed high similarity in both groups.

Having verified the validity of the model, an analysis of the rate constants corresponding to the model's state transitions and their voltage dependence was performed. In Kv1.1 (Fig. 8a), the voltage dependence of the rate constants of all transitions was fitted well with single-exponential functions. Forward transitions had larger rate constants and exhibited stronger voltage dependence (z values) than the corresponding backward transitions. Notably, analysis of the rate constants in Kv1.1+syx (Fig. 8b) revealed several dramatic differences from Kv1.1. First, several transitions ($C_n \leftrightarrow S2$, $C_n \leftrightarrow F$ and $S1 \leftrightarrow F$) had rate constants of no considerable magnitude, rendering these transitions relatively insignificant. Second, some forward transitions had smaller rate constants than the corresponding backward transition (in $C_n \leftrightarrow S1$ and $S1 \leftrightarrow S2$). Third, the voltage dependence of the rate constants of the significant transitions was complex and could be fitted only with the exponential product function (Eq. (2)), namely, a biphasic dependence of the rate constants on voltage.

Impact of the interaction of Kv1.1 with syx on neuronal physiology

What may be the possible influence of the interaction of Kv1.1 with syx on neuronal physiology? To address this question, we constructed a simplified biophysical model of Kv1.1 and Kv1.1+syx based on the analysis of currents recorded from macro patches and simulated action potential generation. The model consisted of a single compartment simulating a spherical cell with one type of each voltage-gated sodium and potassium channels. The model was loosely based on the model for action potential generation in the giant squid axon [28–30]. The voltage-gated potassium conductance in our model had a membrane density of 200 pS/μm^2, and the kinetics of the delayed rectifier potassium conductance from the original Hodgkin–Huxley (H–H) model was replaced with the kinetics of Kv1.1 (Fig. 6c). The voltage-gated Na^+ conductance had in our model the same kinetics of the original H–H model with a membrane density of 500 pS/m^2. We also performed several simulations using voltage-gated Na^+ channel kinetics extracted from cortical pyramidal neurons [31] producing qualitatively similar results to those obtained using the kinetics of the original H–H model. The response of this simulated spherical neuron to graded levels of current injection is shown in Fig. 9a. Similarly to the original H–H model (1952), current injection resulted in a regular train of action potentials at a constant frequency that increased with the amount of injected current (Fig. 9a). The simulation postulated that only 25% of Kv1.1 channels are associated with syx. Thus, the conductance density of free Kv1.1 model was reduced to 150 pS/μm^2 and a model of the Kv1.1 interacting with syx, based on the information presented in Fig. 6a–c, was added to the simulation with a conductance density of 25 pS/μm^2 (a twofold reduction in conductance based on Fig. 4a showing that co-expression of Kv1.1 with syx decreased the single channel conductance by 50%). Similar levels of current injection failed to produce action potential trains or produced trains with a lower firing frequency than that obtained when no syx was inserted into the model (Fig. 9b). Analysis of several levels of current injections showed that the inclusion of the Kv1.1

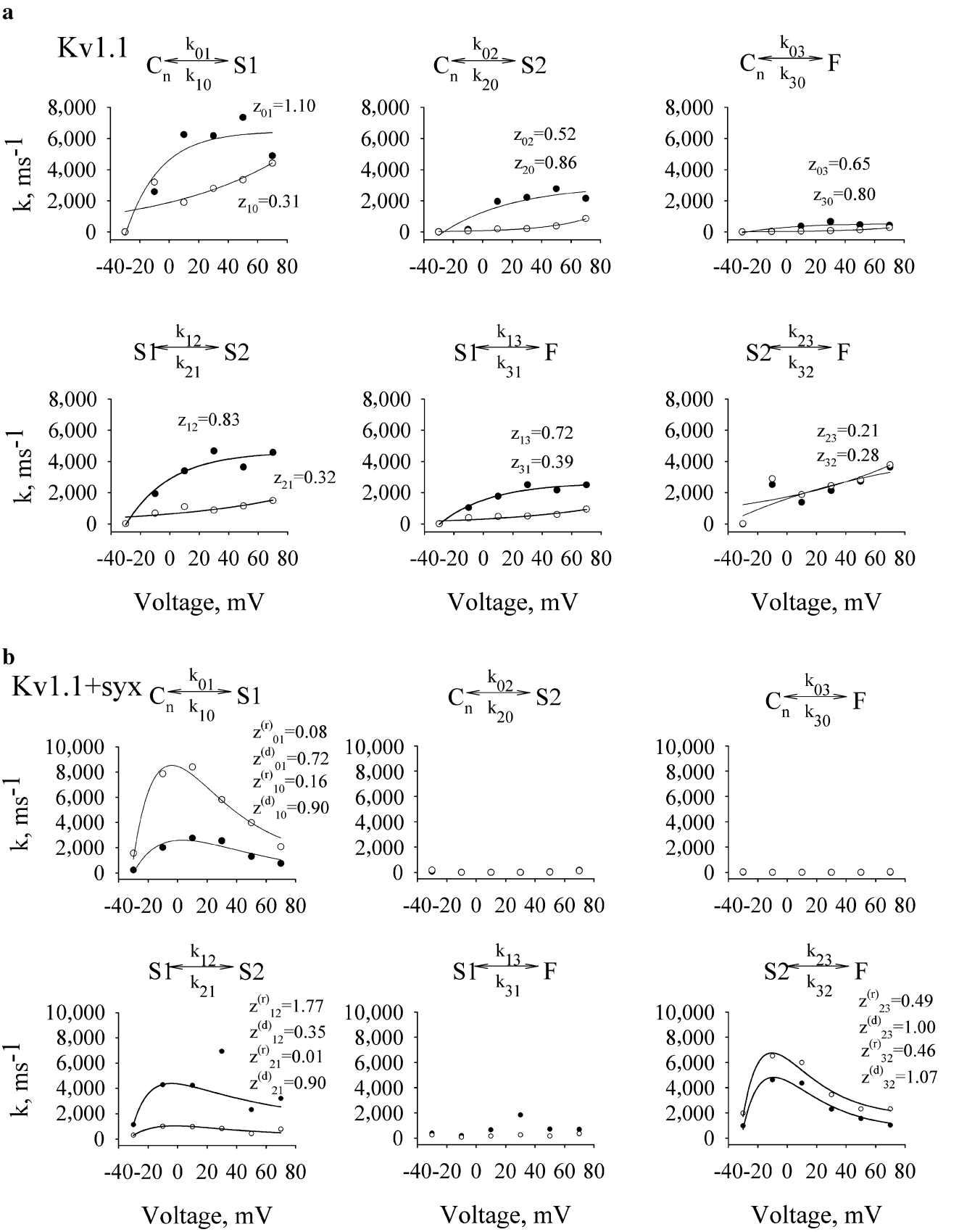

Fig. 8 State transition rate constants for Kv1.1 and Kv1.1+syx and their voltage dependence. The rate constants of Kv1.1 and Kv1.1+syx were fitted with one-exponential and exponential product functions, respectively; the derived *z* values, the charge transfer in e^0 units per subunit, are depicted for each transition. *Closed* and *open circles* depict $i \rightarrow j$ (forward) and $j \rightarrow i$ (backward) state transition rate constants, respectively

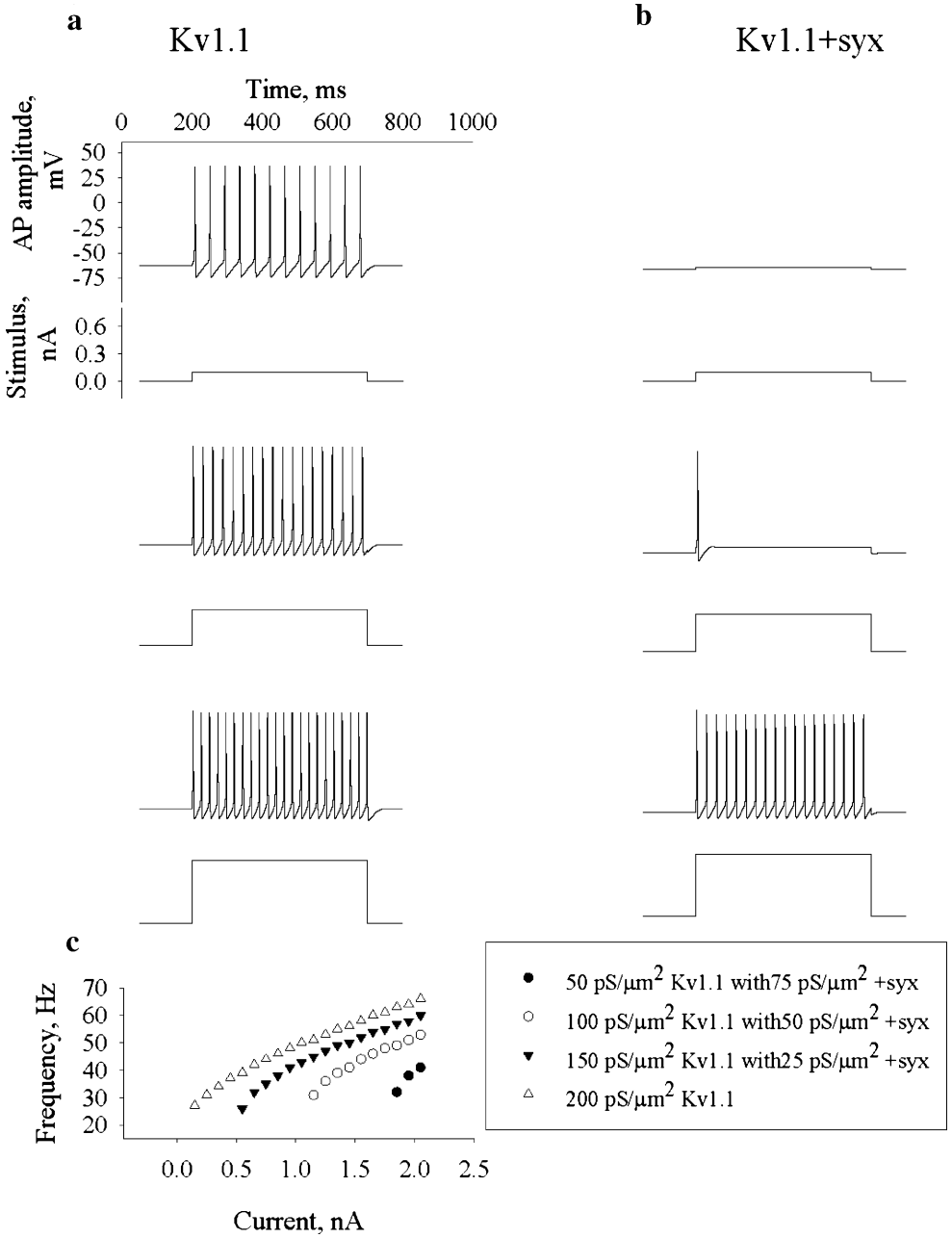

Fig. 9 Interaction of Kv1.1 with syx shifts the F–I curve. Action potential simulations. **a** The response of a H–H model in which the delayed rectifier potassium conductance model was replaced with a model of Kv1.1 to several levels of 500 ms current injections. **b** The response of the same model in which 50 pS/μm^2 of the Kv1.1 model were replaced with 25 pS/μm^2 of the model for Kv1.1 co-expressed with syx. The scale bar applies to all the presented traces. **c** The dependence of the frequency of a train of action potentials on the injected current is displayed for several combinations of Kv1.1 and Kv1.1 interacting with syx. 200 pS/μm^2 Kv1.1 (*closed circles*), 150 pS/μm^2 Kv1.1 with 25 pS/μm^2 Kv1.1+syx (*closed squares*), 100 pS/μm^2 Kv1.1 with 50 pS/μm^2 Kv1.1+syx (*closed triangles*), and 50 pS/μm^2 Kv1.1 with 75 pS/μm^2 Kv1.1+syx (*closed diamonds*). The firing frequency was not calculated for membrane potential traces that displayed only a single AP

interaction with syx into the model resulted in a shift in the frequency–current (*F–I*) curve to higher levels of injected current (Fig. 9c). The larger the fraction of the Kv1.1 conductance that was replaced with a syx-interacting Kv1.1, the greater was the shift in the *F–I* curve (Fig. 9c).

Discussion

In this study, we provide significant insights into the mechanism underlying the regulation of Kv1.1 by syx. Syx affects both P_o and γ to yield a dual effect on macroscopic conductance: a massive decrease at potentials above threshold that is inverted into an enhancement at threshold potentials. Kinetic analysis followed by modeling highlights a mechanism whereby syx achieves tight control over the activation gating by enabling only a single pathway for state transitions from closed to fully-open state, via a sequence of subconductance states. The dual effect of syx on macroscopic conductance may result in shunting inhibition in neurons, in accord with the proposed role for Kv1.1 in axonal excitability and synaptic efficacy. Altogether, we suggest a mechanism to modulate the gain of neuronal output in response to different levels of syx.

Effects of syx on a single Kv1.1 channel

Analysis of unitary steady state activation parameters γ and P_o showed that syx reduced maximal macroscopic conductance by ~50%, shifted $V_{1/2}$ to more hyperpolarized potentials and reduced the voltage sensitivity (Fig. 4a–d). The changes in the voltage dependence (demonstrated also by analysis of macroscopic currents; Fig. 6a,b) were due to corresponding changes observed only in S1 and S2 levels (Fig. 3), of which the relative contributions increased significantly at potentials near the threshold of activation (Fig. 4e). This is in accord with the *Shaker* B channel where subconductances have substantial contribution at threshold potentials [32, 33]. Further, kinetic analysis (Fig. 5) of the single channel behavior showed that only closed time, but not open time, behavior could account for the lower P_o observed in Kv1.1+syx patches due to significant prolongation of mean closed times at all potentials. It is important to note that the total mean open time, but not the mean closed time was increased dramatically at −30 mV by syx. Assuming that this trend also holds at more negative potentials, it may underlie the hyperpolarizing shift in activation caused by syx (Fig. 4b). In support, channel openings were observed at −50 mV only in Kv1.1+syx patches (Fig. 1).

A mechanism whereby syx reduces macroscopic conductance through a decrease in P_o, resulting from prolonged mean-closed time, was suggested for the epithelial sodium channel [34]. However, with Kv1.1, syx integrates two means to effectively reduce the macroscopic conductance; in addition to the decrease in P_o, syx decreases also γ. Moreover, in the case of a voltage-gated channel like Kv1.1, syx also affects the voltage dependence of P_o to further shape excitability.

Proposed mode of action of syx

Based on the kinetic data, simplified kinetic models of state transitions for Kv1.1, alone and in the presence of syx, were suggested (Fig. 7a) and further validated by the high resemblance between the simulated and the experimental data analyses (Fig. 7). Only in Kv1.1 alone the simulated rate constants of transitions between the last closed state before opening (C_n) and each of the three conductance states are significant, rendering the transitions energetically favorable; the transition $C_n \leftrightarrow F$ is the least energetically favorable (Fig. 8a). All transitions in Kv1.1 show one-exponent voltage dependence. Noticeably, in all transitions (except $S2 \leftrightarrow F$) the on-rates (from lower to higher conductance) are higher and more voltage-dependent than the corresponding off-rates. Thus, the depolarization-induced activation of the channel is favored.

In the presence of syx (Fig. 8b), three prominent major phenomena highlight the modus operandi of syx, as illustrated in the state transitions models for Kv1.1, alone and in the presence of syx (Fig. 10). First, only one pathway for state transitions, $C_n \leftrightarrow S1 \leftrightarrow S2 \leftrightarrow F$, has a significant contribution to the single-channel behavior in the presence of syx. Secondly, in the transition $C_n \leftrightarrow S1$, the first in the sequential channel opening, the on-rate is lower than the off-rate at all voltages, suggesting that this is the rate-limiting step for opening in the presence of syx, leading to stabilization of the closed state by increasing the energy barrier for opening. This predicts for Kv1.1+syx a prolongation of closed dwell times (Fig. 5e), leading to decreased P_o and lower maximal macroscopic conductance (Fig. 4a), but is in an apparent contradiction to the openings at −50 mV (Fig. 1). This discrepancy is resolved by considering Le Chatelier's principle, according to which the probability of openings is greatly dependent on the absolute values of α and β (the on-rate and off-rate for all the closed states before the first opening, correspondingly) and on the ratio α/β (reflected in MFL). Indeed, the observed and simulated MFLs at negative potentials become shorter (α/β larger) in the presence of syx (Figs. 6e and 7f, respectively). This argues for a significant alleviation of state transition from closed to open at more negative potentials, which possibly underlies the leftward-shift of the activation curve by syx (Figs. 4b and 6b).

The third prominent phenomenon by syx is the compound voltage-dependence of the state transition rate constants suggesting contribution from two voltage-dependent processes: acceleration of rates with increasing voltages up to +10 mV that is replaced by deceleration at more positive potentials, arguing for a voltage-dependent interaction of syx with the channel. Further, the off-rate constant of the limiting step $C_n \leftrightarrow S1$ decelerates much more significantly than its on-rate constant (the equilibrium constant (k_{off}/k_{on}) is

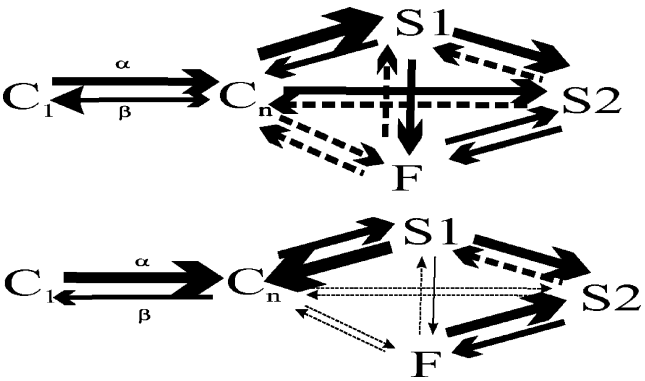

Fig. 10 State transitions model for Kv1.1 alone and in the presence of syx. Syx turns off all transitions except for $C_n \leftrightarrow S1 \leftrightarrow S2 \leftrightarrow F$, enhances the off-rate of the first opening transition ($C_n \leftrightarrow S1$) and increases the ratio of α/β. *Solid lines* depict fast transitions (width of the line is proportional to the rate)

therefore reduced from 3.04 at +10 mV to 2.8 at +70 mV), suggesting that at positive potentials the energetic barrier for opening, imposed by syx, is somewhat relieved. Notably, previously we demonstrated in fresh brain synaptosomes that the physical interaction between Kv1.1 and syx was attenuated after depolarization by KCl [10].

Recently, a model for the activation of another Kv channel (Kv2.1) harboring subconductances, resulting from heteromeric pore conformations, was proposed [35]. In this model channel opening involves a sequence of discrete sublevels through which the permeation rate increases incrementally to reach the fully-open level. The sublevels are partially activated channels where one or more voltage sensors have activated. Further, activation and channel opening were claimed to be allosterically coupled [36]. Our model for Kv1.1, unlike the Kv2.1 model, harbors, in addition to sequential transitions, also non-sequential transitions (*e.g.*, $S1 \leftrightarrow F$). It is quite possible that we failed to detect intermediate sequential transitions of extremely short dwell-times. Such suppression of intermediates, a feature of allosteric interactions, indicates that the transitions are highly cooperative, likely indicating quite tight packing of Kv1.1 subunits at the central pore region.

Notably, in the model for Kv1.1 in the presence of syx, transitions from closed to fully-open state are forced only via sequence of discrete substates, suggesting that syx causes breakdown of some cooperative movements of the voltage sensors, possibly via loosening the tight packing of subunits. This is supported by the reduced slope of activation in the presence of syx (Fig. 4b). Further, the Kv2.1 model suggests that at threshold, where channels spend a long time in the subconductances, cooperativity may break down. Indeed, the Kv1.1 unitary events, observed at −50 mV only in the presence of syx, together with the significant increase in the relative contribution of S1, at the expense of F (Fig. 4e), further attests that the interaction of syx with the channel can direct cooperativity breakdown.

Altogether, syx gains efficient control over the activation of Kv1.1 by primarily restricting the channel opening to a single conduction pathway, very likely via breaking down cooperativity. To achieve attenuation of activation at potentials above threshold, syx restrains the first transition in this pathway, from closed to S1, by increasing the energy barrier for the on-reaction. To obtain openings at threshold potentials, syx increases the ratio α/β.

In a structural context, the dependence of the interaction between syx and the channel on voltage corroborates our previous suggestion that this interaction is due to a membrane delimited physical interaction between the proteins [10]. The question arises how changes in both gating and pore properties can be reconciled with the previous findings [17] that syx binds the N-terminus, specifically the T1 domain, of Kv1.1? It was proposed that the N-terminus of Kv1 channels is coupled both to voltage-dependent gating and pore region properties. Hence, structural alterations of the T1 domain of Kv1.1 affect gating properties, manifested in shifts of activation curves and altered channel closing rates, analogous to the above described effect of syx on Kv1.1 gating [37]. Additionally, mutations at the N-terminus of Kv1.3 modulate the affinity of channel blockers to the extracellular surface of the pore and increase single-channel conductance [38]. Recently, compelling evidence for a tight coupling between voltage-dependent activation of a Kv4 channel and conformational changes in the intracellular T1–T1 interface was provided [39]. Such interplay between plasma membrane and intracellular factors in the control of potassium channel activities has been suggested as a possible means of communication between second messenger pathways and Kv channels [40].

Syx increases K^+ current close to resting membrane potential and reduces the excitability of neurons

Integration of the data into the simple model of action potential generation, based on the model of the squid giant axon, revealed that the larger the fraction of the Kv1.1 conductance that was replaced with a syx-interacting Kv1.1, the more was the frequency–current curve shifted to higher current values. This reduction in neuronal excitability is probably due to the major effect of syx on the steady-state activation curve, which shifts it to hyperpolarized potentials (Figs. 4b and 6b). This effect results in greater channel activation at subthreshold potentials, resulting in an increased membrane shunt that may act as local or global inhibition of synaptic input. While the syx enhancing effect on activation and deactivation kinetics seems large, it is limited to a small range of voltages (Fig. 6c). Consequently, syx does not affect the amplitude or the shape of the action potential waveform. Thus, shunting potassium conductance at subthreshold potentials reduces the excitability of the neuron and may result in a smaller release probability at the presynaptic terminals. Indeed, several studies addressed to evaluate the role of Kv1.1 in axonal excitability and synaptic efficacy, indicate a role in firing frequency [15, 41–43]. Taken together, we hypothesize that this mechanism may serve to modulate the gain of neuronal output and synaptic activity in response to different levels of syx.

It is important to point out that the model we present here was constructed using only the activation and deactivation properties of Kv1.1 and Kv1.1+syx without taking into account processes of inactivation. However, fast inactivation occurs upon association of Kv1.1 with Kvβ1 subunits [44] and its extent is increased by interaction with syx [10]. Co-localization of Kv1.1 with Kvβ1 was demonstrated in synaptic terminals in specific regions of

rodent brain including Hippocampal Mossy Fiber Boutons [1, 45]. In the latter case, inactivation of Kv1 channels was proposed to take part in spike broadening [46]. Thus it is possible that the interaction of syx with Kv1.1 at sites of co-localization with Kvβ1 has a duel effect: reducing excitability by increasing the K^+ shunt and increasing release probability by enhancing Kv1.1 inactivation that causes spike broadening. The two effects, combined, lead to a more efficient release.

Further thoughts

Syx may exert dual regulation of the Kv1.1 channel activity. The same concentration of syx that downregulated the single channel activity in this study was shown by us to increase whole cell currents recorded by two-electrode voltage clamp [10], implying an enhanced, syx-driven, channel trafficking to the plasma membrane, which overrides the decrease in channel conductivity (Moskovitz et al. in preparation). In accord, the pronounced clustering behavior upon coexpression of syx, observed in the patch clamp experiments, argues in favor of better fusion of intracellular vesicles with the plasma membrane, induced by syx, to enhance the cell surface insertion of Kv channels. This may constitute a second pathway for syx to up-regulate whole cell channel function and pattern of expression at discrete spots of vesicle fusion. This dual regulation of Kv1.1 surface activity by syx argues for a dynamic control of neuronal excitability and possibly of presynaptic events.

Acknowledgements This work was supported by a grant from the Israel Academy of Sciences (I.L.).

References

1. Veh RW, Lichtinghagen R, Sewing S, Wunder F, Grumbach IM, Pongs O (1995) Immunohistochemical localization of five members of the Kv1 channel subunits: contrasting subcellular locations and neuron-specific co-localizations in rat brain. Eur J Neurosci 7:2189–2205
2. Wang H, Allen ML, Grigg JJ, Noebels JL, Tempel BL (1995) Hypomyelination alters K+ channel expression in mouse mutants shiverer and Trembler. Neuron 15:1337–1347
3. Rasband MN, Trimmer JS, Schwarz TL, Levinson SR, Ellisman MH, Schachner M, Shrager P (1998) Potassium channel distribution, clustering, and function in remyelinating rat axons. J Neurosci 18: 36–47
4. Wang H, Kunkel DD, Martin TM, Schwartzkroin PA, Tempel BL (1993) Heteromultimeric K+ channels in terminal and juxtaparanodal regions of neurons. Nature 365:75–79
5. Wang H, Kunkel DD, Schwartzkroin PA, Tempel BL (1994) Localization of Kv1.1 and Kv1.2, two K channel proteins, to synaptic terminals, somata, and dendrites in the mouse brain. J Neurosci 14:4588–4599
6. Grissmer S, Nguyen AN, Aiyar J, Hanson DC, Mather RJ, Gutman GA, Karmilowicz MJ, Auperin DD, Chandy KG (1994) Pharmacological characterization of five cloned voltage-gated K+ channels, types Kv1.1, 1.2, 1.3, 1.5, and 3.1, stably expressed in mammalian cell lines. Mol Pharmacol 45:1227–1234
7. Stuhmer W, Ruppersberg JP, Schroter KH, Sakmann B, Stocker M, Giese KP, Perschke A, Baumann A, Pongs O (1989) Molecular basis of functional diversity of voltage-gated potassium channels in mammalian brain. EMBO J 8:3235–3244
8. Meiri N, Ghelardini C, Tesco G, Galeotti N, Dahl D, Tomsic D, Cavallaro S, Quattrone A, Capaccioli S, Bartolini A, Alkon DL (1997) Reversible antisense inhibition of Shaker-like Kv1.1 potassium channel expression impairs associative memory in mouse and rat. Proc Natl Acad Sci USA 94:4430–4434
9. Shillito P, Molenaar PC, Vincent A, Leys K, Zheng W, van den Berg RJ, Plomp JJ, van Kempen GT, Chauplannaz G, Wintzen AR et al (1995) Acquired neuromyotonia: evidence for autoantibodies directed against K+ channels of peripheral nerves. Ann Neurol 38:714–722
10. Fili O, Michaelevski I, Bledi Y, Chikvashvili D, Singer-Lahat D, Boshwitz H, Linial M, Lotan I (2001) Direct interaction of a brain voltage-gated K+ channel with syntaxin 1A: functional impact on channel gating. J Neurosci 21:1964–1974
11. Bajjalieh SM, Scheller RH (1995) The biochemistry of neurotransmitter secretion. J Biol Chem 270:1971–1974
12. Sudhof TC (1995) The synaptic vesicle cycle: a cascade of protein–protein interactions. Nature 375:645–653
13. Linial M, Parnas D (1996) Deciphering neuronal secretion: tools of the trade. Biochim Biophys Acta 1286:117–152
14. Bennett MK (1995) SNAREs and the specificity of transport vesicle targeting. Curr Opin Cell Biol 7:581–586
15. Lopantsev V, Tempel BL, Schwartzkroin PA (2003) Hyperexcitability of CA3 pyramidal cells in mice lacking the potassium channel subunit Kv1.1. Epilepsia 44:1506–1512
16. Sheng ZH, Rettig J, Cook T, Catterall WA (1996) Calcium-dependent interaction of N-type calcium channels with the synaptic core complex. Nature 379:451–454
17. Michaelevski I, Chikvashvili D, Tsuk S, Fili O, Lohse MJ, Singer-Lahat D, Lotan I (2002) Modulation of a brain voltage-gated K+ channel by syntaxin 1A requires the physical interaction of Gbetagamma with the channel. J Biol Chem 277:34909–34917
18. Jarvis SE, Magga JM, Beedle AM, Braun JE, Zamponi GW (2000) G protein modulation of N-type calcium channels is facilitated by physical interactions between syntaxin 1A and Gbetagamma. J Biol Chem 275:6388–6394
19. Jarvis SE, Zamponi GW (2001) Distinct molecular determinants govern syntaxin 1A-mediated inactivation and G-protein inhibition of N-type calcium channels. J Neurosci 21:2939–2948
20. Bezprozvanny I, Zhong P, Scheller RH, Tsien RW (2000) Molecular determinants of the functional interaction between syntaxin and N-type Ca2+ channel gating. Proc Natl Acad Sci USA 97:13943–13948
21. Stanley EF, Mirotznik RR (1997) Cleavage of syntaxin prevents G-protein regulation of presynaptic calcium channels. Nature 385:340–343
22. Dascal N, Lotan I, Karni E, Gigi A (1992) Calcium channel currents in Xenopus oocytes injected with rat skeletal muscle RNA. J Physiol 450:469–490
23. Singer-Lahat D, Dascal N, Lotan I (1999) Modal behavior of the Kv1.1 channel conferred by the Kvbeta1.1 subunit and its regulation by dephosphorylation of Kv1.1. Pflugers Arch 439:18–26
24. Hines ML, Carnevale NT (1997) The NEURON simulation environment. Neural Comput 9:1179–1209
25. Islas LD, Sigworth FJ (1999) Voltage sensitivity and gating charge in Shaker and Shab family potassium channels. J Gen Physiol 114:723–742

26. Qin F, Auerbach A, Sachs F (1997) Maximum likelihood estimation of aggregated Markov processes. Proc Biol Sci 264:375–383
27. Qin F, Auerbach A, Sachs F (2000) Hidden Markov modeling for single channel kinetics with filtering and correlated noise. Biophys J 79:1928–1944
28. Hodgkin AL, Huxley AF (1952) Propagation of electrical signals along giant nerve fibers. Proc R Soc Lond B Biol Sci 140:177–183
29. Hodgkin AL, Huxley AF (1952) Movement of sodium and potassium ions during nervous activity. Cold Spring Harb Symp Quant Biol 17:43–52
30. Hodgkin AL, Huxley AF, Katz B (1952) Measurement of current–voltage relations in the membrane of the giant axon of Loligo. J Physiol 116:424–448
31. Keren N, Peled N, Korngreen A (2005) Constraining compartmental models using multiple voltage recordings and genetic algorithms. J Neurophysiol 94:3730–3742
32. Zheng J, Sigworth FJ (1997) Selectivity changes during activation of mutant Shaker potassium channels. J Gen Physiol 110:101–117
33. Zheng J, Sigworth FJ (1998) Intermediate conductances during deactivation of heteromultimeric Shaker potassium channels. J Gen Physiol 112:457–474
34. Condliffe SB, Zhang H, Frizzell RA (2004) Syntaxin 1A regulates ENaC channel activity. J Biol Chem 279:10085–10092
35. Chapman ML, Vandongen AM (2005) K channel subconductance levels result from heteromeric pore conformations. J Gen Physiol 126:87–103
36. Bezanilla F (2005) The origin of subconductance levels in voltage-gated K+ channels. J Gen Physiol 126:83–86
37. Cushman SJ, Nanao MH, Jahng AW, DeRubeis D, Choe S, Pfaffinger PJ (2000) Voltage dependent activation of potassium channels is coupled to T1 domain structure. Nat Struct Biol 7:403–407
38. Yao X, Liu W, Tian S, Rafi H, Segal AS, Desir GV (2000) Close association of the N terminus of Kv1.3 with the pore region. J Biol Chem 275:10859–10863
39. Wang G, Covarrubias M (2006) Voltage-dependent gating rearrangements in the intracellular T1–T1 interface of a K+ channel. J Gen Physiol 127:391–400
40. Yi BA, Minor DL Jr, Lin YF, Jan YN, Jan LY (2001) Controlling potassium channel activities: Interplay between the membrane and intracellular factors. Proc Natl Acad Sci USA 98:11016–11023
41. Chiu SY, Zhou L, Zhang CL, Messing A (1999) Analysis of potassium channel functions in mammalian axons by gene knockouts. J Neurocytol 28:349–364
42. Tan YP, Llano I (1999) Modulation by K+ channels of action potential-evoked intracellular Ca2+ concentration rises in rat cerebellar basket cell axons. J Physiol 520 Pt 1:65–78
43. Dodson PD, Barker MC, Forsythe ID (2002) Two heteromeric Kv1 potassium channels differentially regulate action potential firing. J Neurosci 22:6953–6961
44. Rettig J, Heinemann SH, Wunder F, Lorra C, Parcej DN, Dolly JO, Pong O (1994) Inactivation properties of voltage-gated K+ channels altered by presence of beta-subunit. Nature 369:289–294
45. Rhodes KJ, Keilbaugh SA, Barrezueta NX, Lopez KL, Trimmer JS (1995) Association and colocalization of K+ channel alpha- and beta-subunit polypeptides in rat brain. J Neurosci 15:5360–5371
46. Geiger JR, Jonas P (2000) Dynamic control of presynaptic Ca(2+) inflow by fast-inactivating K(+) channels in hippocampal mossy fiber boutons. Neuron 28:927–939